INSTITUTE OF MATHEMATICS

THE CZECH ACADEMY OF SCIENCES

New invariant domain preserving finite volume schemes for compressible flows

Mária Lukáčová-Medviďová

Hana Mizerová

Bangwei She

New Invariant Domain Preserving Finite Volume Schemes for Compressible Flows

M. Lukáčová-Medviďová, Hana Mizerová, and Bangwei She

Abstract We present new invariant domain preserving finite volume schemes for the compressible Euler and Navier–Stokes–Fourier systems. The schemes are entropy stable and preserve positivity of density and internal energy. More importantly, their convergence towards a strong solution of the limit system has been proved rigorously in [9, 11]. We will demonstrate their accuracy and robustness on a series of numerical experiments.

Key words: compressible Euler and Navier–Stokes–Fourier systems, finite volume methods, invariant domain preserving properties, entropy stability, convergence

M. Lukáčová-Medviďová
Institute of Mathematics, Johannes Gutenberg-University Mainz, Staudingerweg 9, 55 128 Mainz, Germany, e-mail: lukacova@uni-mainz.de

Hana Mizerová
Institute of Mathematics of the Czech Academy of Sciences, Žitná 25, CZ-115 67 Praha 1, Czech Republic;
Department of Mathematical Analysis and Numerical Mathematics, Faculty of Mathematics, Physics and Informatics of the Comenius University, Mlynská dolina, 842 48 Bratislava, Slovakia, e-mail: hana.mizerova@fmph.uniba.sk

Bangwei She
Institute of Mathematics of the Czech Academy of Sciences, Žitná 25, CZ-115 67 Praha 1, Czech Republic, e-mail: she@math.cas.cz

1

1 Introduction

Numerical simulations of compressible flows find their applications in many everyday problems, ranging from engineering, oceanography, meteorology to hemodynamics. Over the years a large variety of powerful numerical schemes has been developed. Let us point out a few well-established and practical schemes, e.g., [1, 5, 6, 12, 16, 18, 19, 23, 25]. Despite of their practical success the rigorous numerical analysis, in particular, in multiple space dimensions, is still open in general.

In [13, 14] the concept of *invariant domain preserving schemes* for hyperbolic conservation laws has been introduced. These methods satisfy some important structure preserving properties, such as positivity of some quantities, entropy production or the minimum entropy principle. In our recent works [9, 10, 11] we have proposed new finite volume schemes for the compressible Euler equations of gas dynamics, compressible Navier–Stokes and Navier–Stokes–Fourier equations, respectively. Our new finite volume methods belong to the class of the invariant domain preserving schemes. Their properties further allowed us to study the convergence of the schemes rigorously. More precisely, we proved a nonlinear variant of the *Lax equivalence theorem*: a consistent numerical scheme is convergent if and only if it is stable.

Of course, the compressible Euler and Navier–Stokes–Fourier equations are truly nonlinear, thus we have to overcome difficulties arising due to nonlinear terms. To this goal, we apply a concept of dissipative measure–valued solutions developed in [2, 3, 8] for the above mentioned systems, respectively. Indeed, the Young measures which are the space-time parametrized probability measures replace the linearity setting. They allow us to pass to the limit in nonlinear terms and show the convergence of our finite volume schemes. A limit is in general only a measure, more precisely a dissipative measure–valued solution. We refer a reader to [2, 3, 8] and [9, 10, 11] for more details on its definition.

A crucial ingredient of our convergence analysis is the fact that we have the weak-strong uniqueness principle for all systems mentioned above. More precisely, if the strong solution exists our dissipative measure–valued solution coincides with the former on its lifespan. Consequently, we get the strong convergence of our numerical solutions to the strong solution in appropriate Lebesgue spaces. The main aim of this paper is to illustrate experimentally the behaviour of our new invariant domain preserving finite volume schemes for compressible fluids, namely for the Euler and the Navier–Stokes–Fourier systems, cf. [9, 11].

The gas dynamics of inviscid compressible flows is governed by the Euler equations

$$\partial_t \varrho + \mathrm{div}_x \boldsymbol{m} = 0,$$
$$\partial_t \boldsymbol{m} + \mathrm{div}_x (\boldsymbol{m} \otimes \boldsymbol{u}) + \nabla_x p = 0,$$
$$\partial_t E + \mathrm{div}_x ((E + p)\boldsymbol{u}) = 0, \tag{1}$$

where $\varrho, p, \boldsymbol{u}, \boldsymbol{m} = \varrho\boldsymbol{u}$, and E represent the density, pressure, velocity, momentum and the total energy of a fluid, respectively. Taking into account the viscous and heat conducting effects yields the Navier–Stokes–Fourier equations

$$\partial_t \varrho + \text{div}_x \boldsymbol{m} = 0,$$
$$\partial_t \boldsymbol{m} + \text{div}_x(\boldsymbol{m} \otimes \boldsymbol{u}) + \nabla_x p = \text{div}_x \mathbb{S}(\mathbf{D}(\boldsymbol{u})),$$
$$\partial_t(\varrho e) + \text{div}_x(\varrho e \boldsymbol{u}) - \text{div}_x(\kappa \nabla_x \vartheta) = \mathbb{S}(\mathbf{D}(\boldsymbol{u})) : \nabla_x \boldsymbol{u} - p \text{div}_x \boldsymbol{u}, \qquad (2)$$

where the viscous stress tensor $\mathbb{S}$ reads

$$\mathbb{S}(\mathbf{D}(\boldsymbol{u})) = 2\mu\mathbf{D}(\boldsymbol{u}) + \lambda\text{div}_x\boldsymbol{u}\mathbb{I}, \quad \mathbf{D}(\boldsymbol{u}) = \frac{\nabla_x\boldsymbol{u} + \nabla_x\boldsymbol{u}^T}{2}.$$

The systems (1) and (2) are closed by the standard pressure law for a perfect gas $p = p(\varrho, \vartheta) = \varrho\vartheta$, ϑ is the temperature. Denoting further e the specific internal energy, s the physical entropy, $\gamma > 1$ the adiabatic coefficient and $c_v = \frac{1}{\gamma-1}$ the specific heat at constant volume we have

$$e(\varrho, \vartheta) = c_v\vartheta, \ s(\varrho, \vartheta) = \log\left(\frac{\vartheta^{c_v}}{\varrho}\right) = \frac{1}{\gamma-1}\log\left(\frac{p}{\varrho^\gamma}\right).$$

The total energy $E = \frac{1}{2}\frac{\boldsymbol{m}^2}{\varrho} + \varrho e$ consists of the kinetic energy and the internal energy.

Both systems (1) and (2) are solved in the time-space cylinder $(0, T) \times \Omega, \Omega \subset R^d$, $d = 2, 3$. We assume that these systems are accompanied with appropriate boundary conditions: either the periodic boundary conditions when the domain Ω is identified with a flat torus, or the no flux boundary conditions,

$$\boldsymbol{u}|_{\partial\Omega} \cdot \boldsymbol{n} = 0, \ \nabla_x\vartheta \cdot \boldsymbol{n} = 0$$

in the case of the Euler equations (1), or the no–slip boundary conditions,

$$\boldsymbol{u}|_{\partial\Omega} = 0$$

for the Navier–Stokes–Fourier system (2). To close the formulation of the problem we impose the initial conditions

$$\mathbf{U}(0) = \mathbf{U}_0, \ \text{with } \varrho_0 > 0 \text{ and } E_0 - \frac{1}{2}\frac{|\boldsymbol{m}_0|^2}{\varrho_0} > 0, \qquad (3)$$

where $\mathbf{U} = (\varrho, \boldsymbol{m}, E)$ or $\mathbf{U} = (\varrho, \boldsymbol{m}, \vartheta)$ for the Euler and the Navier–Stokes–Fourier equations, respectively.

2 Finite Volume Schemes

We start by introducing the mesh, space discretization and suitable discrete spaces.

2.1 Mesh and Space Discretization

Primary grid. We suppose the physical space to be a polyhedral domain $\Omega \subset R^d$, $d = 2, 3$, that is decomposed into compact elements,

$$\overline{\Omega} = \bigcup_{K \in \mathcal{T}_h} K.$$

The elements K are sharing either a common face, edge, or vortex.

They can be chosen to be triangular, rectangular, or any combination of them. The primary mesh $\mathcal{T}_h$ is assumed to satisfy the standard regularity assumptions, cf. [4, 7]. The set of all faces is denoted by Σ, while the set of faces on the boundary is denoted by Σ_{ext}, and the set of interior faces by $\Sigma_{int} = \Sigma \backslash \Sigma_{ext}$. Note that there is no boundary if the flow is periodic:

$$\Sigma_{ext} = \emptyset \ \text{ and } \ \Sigma_{int} = \Sigma.$$

Each face is associated with an outer normal vector $\boldsymbol{n}$. Let $|K|$, $|\sigma|$ be the Lebesgue measure of an element K and a face σ, respectively. We shall suppose

$$|K| \approx h^d, \ |\sigma| \approx h^{d-1} \text{ for any } K \in \mathcal{T}_h, \ \sigma \in \Sigma.$$

The parameter $h \in (0, 1)$ is the maximum element size, i.e., the size of the mesh $\mathcal{T}_h$.

For the discretization of the Navier–Stokes–Fourier system (2) we additionally require the primary grid $\mathcal{T}_h$ to satisfy the following property: there is a family of control points $P_h = \{\mathbf{x}_K \,|\, \mathbf{x}_K \in K, K \in \mathcal{T}_h\}$, such that the segment $[\mathbf{x}_K, \mathbf{x}_L]$ for any adjacent elements K and L is perpendicular to their common face $\sigma = K \cap L$. We denote by $d_\sigma = (\mathbf{x}_K, \mathbf{x}_L)$ the Euclidean distance betweens the points $\mathbf{x}_K$ and $\mathbf{x}_L$ in R^d. This requirement is naturally satisfied by any rectangular mesh with P_h being the set of gravity centres of all elements. For a triangular mesh, we can use the well-centred mesh [24], where P_h is the set of circumcentres of all elements.

Dual grid. For the theoretical analysis of our finite volume scheme for the Navier–Stokes–Fourier system it is convenient to introduce a dual mesh $\mathcal{D}_h$. A dual cell D_σ associated to a face $\sigma = K \cap L$ is defined as $D_\sigma = D_{\sigma,K} \cup D_{\sigma,L}$, where $D_{\sigma,K}$ $(D_{\sigma,L})$ is a triangle (tetrahedron) built by $\mathbf{x}_K$ and the common vertices of K and L, see Figure 1 for a two-dimensional example.
Discrete function spaces. We denote by Q_h and W_h the set of piecewise constant functions on the primary grid $\mathcal{T}_h$ and the dual grid $\mathcal{D}_h$, respectively. Moreover,
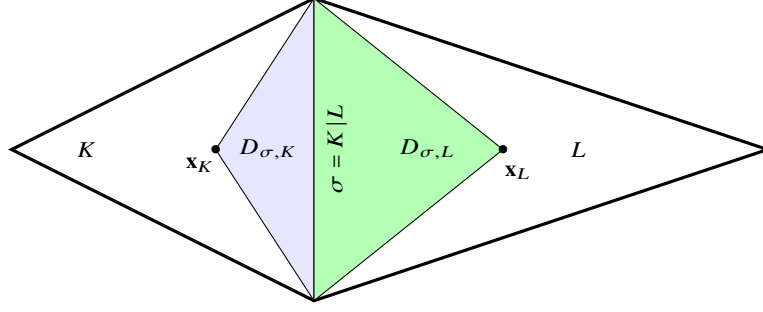
Fig. 1 Dual grid

$v_h \in Q_h$ (resp. $v_h \in W_h$) means that each component of v_h belongs to Q_h (resp. W_h). Further, for a piecewise continuous function v, whenever $x \in \sigma \in \Sigma_{int}$, we define

$$v^{\text{out}}(x) = \lim_{\delta \to 0+} v(x + \delta \boldsymbol{n}), \qquad v^{\text{in}}(x) = \lim_{\delta \to 0+} v(x - \delta \boldsymbol{n}),$$

$$\overline{v}(x) = \frac{v^{\text{in}}(x) + v^{\text{out}}(x)}{2}, \qquad [\![v]\!] = v^{\text{out}}(x) - v^{\text{in}}(x).$$

Upwind flux. Given a velocity $\boldsymbol{u}_h \in Q_h$ and a function $r_h \in Q_h$, we define for each face $\sigma \in \Sigma_{int}$ the upwind flux

$$Up[r_h, \boldsymbol{u}_h] = r_h^{\text{up}} \boldsymbol{u}_h \cdot \boldsymbol{n} = r_h^{\text{in}} [\overline{\boldsymbol{u}_h} \cdot \boldsymbol{n}]^+ + r_h^{\text{out}} [\overline{\boldsymbol{u}_h} \cdot \boldsymbol{n}]^-$$

$$= \overline{r_h} \, \overline{\boldsymbol{u}_h} \cdot \boldsymbol{n} - \frac{1}{2} |\overline{\boldsymbol{u}_h} \cdot \boldsymbol{n}| \, [\![r_h]\!],$$

where

$$[f]^\pm = \frac{f \pm |f|}{2} \quad \text{and} \quad r^{\text{up}} = \begin{cases} r^{\text{in}} & \text{if } \overline{\boldsymbol{u}_h} \cdot \boldsymbol{n} \geq 0, \\ r^{\text{out}} & \text{if } \overline{\boldsymbol{u}_h} \cdot \boldsymbol{n} < 0. \end{cases}$$

Furthermore, we define the numerical flux function

$$F_h(r_h, \boldsymbol{u}_h) = Up[r_h, \boldsymbol{u}_h] - h^\beta \, [\![r_h]\!], \ 0 < \beta < 1.$$

Discrete operators. For any $r_h, v_h \in Q_h$ and $\boldsymbol{q}_h \in W_h$ we define the following discrete gradient and Laplace operators

$$\nabla_{\mathcal{D}} : Q_h \mapsto W_h$$

$$\nabla_{\mathcal{D}} r_h = \sum_{\sigma \in \Sigma} (\nabla_{\mathcal{D}} r_h)_\sigma 1_{D_\sigma}, \quad (\nabla_{\mathcal{D}} r_h)_\sigma = \frac{1}{d_\sigma} [\![r_h]\!] \, \boldsymbol{n},$$

$$\nabla_h : Q_h \mapsto Q_h$$

$$\nabla_h r_h = \sum_{K \in \mathcal{T}_h} (\nabla_h r_h)_K 1_K, \qquad (\nabla_h r_h)_K = \sum_{\sigma \in \partial K} \frac{|\sigma|}{|K|} \overline{r_h} \boldsymbol{n},$$

$$\Delta_h : Q_h \mapsto Q_h$$

$$\Delta_h r_h = \sum_{K \in \mathcal{T}_h} (\Delta_h r_h)_K 1_K, \qquad (\Delta_h r_h)_K = \sum_{\sigma \in \partial K} \frac{|\sigma|}{|K|} \frac{[\![r_h]\!]}{d_\sigma},$$

and discrete divergence operators

$$\mathrm{div}_{\mathcal{T}} : W_h \mapsto Q_h$$

$$\mathrm{div}_{\mathcal{T}} \boldsymbol{q}_h = \sum_{K \in \mathcal{T}_h} (\mathrm{div}_{\mathcal{T}} \boldsymbol{q}_h)_K 1_K, \quad (\mathrm{div}_{\mathcal{T}} \boldsymbol{q}_h)_K = \sum_{\sigma \in \partial K} \frac{|\sigma|}{|K|} \boldsymbol{q}_h \cdot \boldsymbol{n},$$

$$\mathrm{div}_h : Q_h \mapsto Q_h$$

$$\mathrm{div}_h \boldsymbol{v}_h = \sum_{K \in \mathcal{T}_h} (\mathrm{div}_h \boldsymbol{v}_h)_K 1_K, \quad (\mathrm{div}_h \boldsymbol{v}_h)_K = \sum_{\sigma \in \partial K} \frac{|\sigma|}{|K|} \overline{\boldsymbol{v}_h} \cdot \boldsymbol{n},$$

$$\mathrm{div}_h^{\mathrm{up}} : Q_h \mapsto Q_h$$

$$\mathrm{div}_h^{\mathrm{up}}(r_h \boldsymbol{v}_h) = \sum_{K \in \mathcal{T}_h} 1_K \mathrm{div}_h^{\mathrm{up}}(r_h \boldsymbol{v}_h)_K, \quad \mathrm{div}_h^{\mathrm{up}}(r_h \boldsymbol{v}_h)_K = \sum_{\sigma \in \partial K} \frac{|\sigma|}{|K|} F_h(r_h, \boldsymbol{v}_h).$$

Further, the discrete symmetric gradient operator is given by

$$D_h(\boldsymbol{v}_h) = \frac{1}{2}(\nabla_h \boldsymbol{v}_h + \nabla_h^T \boldsymbol{v}_h), \quad \boldsymbol{v}_h \in Q_h.$$

Note that the operators $\nabla_{\mathcal{D}}$ and Δ_h can be extended to vector-valued functions componentwisely. Let $\boldsymbol{v}_h = (v_{1,h}, \dots, v_{d,h}) \in Q_h$. Then we have

$$\nabla_{\mathcal{D}} \boldsymbol{v}_h = (\nabla_{\mathcal{D}} v_{1,h}, \dots, \nabla_{\mathcal{D}} v_{d,h}), \quad \Delta_h \boldsymbol{v}_h = (\Delta_h v_{1,h}, \dots, \Delta_h v_{d,h}),$$

and

$$(\nabla_{\mathcal{D}} \boldsymbol{v}_h)_\sigma = \frac{1}{d_\sigma} [\![\boldsymbol{v}_h]\!] \otimes \boldsymbol{n}, \quad (\Delta_h \boldsymbol{v}_h)_K = \sum_{\sigma \in \partial K} \frac{|\sigma|}{|K|} \frac{[\![\boldsymbol{v}_h]\!]}{d_\sigma}.$$

2.2 Numerical Scheme for the Euler System

We recall a semi-discrete finite volume scheme for the Euler system (1),

$$D_t \varrho_h + \mathrm{div}_h^{\mathrm{up}}(\varrho_h \boldsymbol{u}_h) = 0,$$

$$D_t \boldsymbol{m}_h + \mathrm{div}_h^{\mathrm{up}} F_h(\boldsymbol{m}_h, \boldsymbol{u}_h) + \nabla_h p_h = h^{\alpha-1} \Delta_h \boldsymbol{u}_h,$$

$$D_t E_h + \mathrm{div}_h^{\mathrm{up}} F_h[E_h, \boldsymbol{u}_h] + \boldsymbol{u}_h \cdot \nabla_h p_h + p_h \mathrm{div}_h \boldsymbol{u}_h = \frac{h^{\alpha-1}}{2} \Delta_h(\boldsymbol{u}_h^2),$$

where $\boldsymbol{u}_h = \frac{\boldsymbol{m}_h}{\varrho_h}$, $p_h = (\gamma - 1)\left(E_h - \frac{1}{2}\frac{|\boldsymbol{m}_h|^2}{\varrho_h}\right)$ and D_t stands for the time derivative. The scheme was firstly introduced and studied in its weak form in our recent work [9]. Hereafter we will refer to it as the *FLM method*.

Definition 1 (FLM method) Given the initial values $(\varrho_{0,h}, \boldsymbol{m}_{0,h}, E_{0,h}) \in Q_h \times Q_h \times Q_h$, we seek a piecewise constant approximation $(\varrho_h, \boldsymbol{m}_h, E_h) \in Q_h \times Q_h \times Q_h$ which solves at any time $t \in (0, T]$ the following equations:

$$\int_\Omega D_t \varrho_h \phi_h \, \mathrm{d}x - \sum_{\sigma \in \Sigma_{int}} \int_\sigma F_h(\varrho_h, \boldsymbol{u}_h) \, [\![\phi_h]\!] \, \mathrm{d}S_x = 0, \ \forall \, \phi_h \in Q_h, \qquad (5a)$$

$$\int_\Omega D_t \boldsymbol{m}_h \cdot \boldsymbol{\phi}_h \, \mathrm{d}x - \sum_{\sigma \in \Sigma_{int}} \int_\sigma \mathbf{F}_h(\boldsymbol{m}_h, \boldsymbol{u}_h) \cdot [\![\boldsymbol{\phi}_h]\!] \, \mathrm{d}S_x - \sum_{\sigma \in \Sigma_{int}} \int_\sigma \overline{p_h} \boldsymbol{n} \cdot [\![\boldsymbol{\phi}_h]\!] \, \mathrm{d}S_x$$

$$= -h^{\alpha-1} \sum_{\sigma \in \Sigma_{int}} \int_\sigma [\![\boldsymbol{u}_h]\!] \cdot [\![\boldsymbol{\phi}_h]\!] \, \mathrm{d}S_x, \ \forall \, \boldsymbol{\phi}_h \in Q_h, \quad (5b)$$

$$\int_\Omega D_t E_h \phi_h \, \mathrm{d}x - \sum_{\sigma \in \Sigma_{int}} \int_\sigma F_h(E_h, \boldsymbol{u}_h) \, [\![\phi_h]\!] \, \mathrm{d}S_x - \sum_{\sigma \in \Sigma_{int}} \int_\sigma \overline{p_h} \, [\![\phi_h \boldsymbol{u}_h]\!] \cdot \boldsymbol{n} \mathrm{d}S_x$$

$$+ \sum_{\sigma \in \Sigma_{int}} \int_\sigma \overline{p_h \phi_h} \, [\![\boldsymbol{u}_h]\!] \cdot \boldsymbol{n} \mathrm{d}S_x = -\frac{h^{\alpha-1}}{2} \sum_{\sigma \in \Sigma_{int}} \int_\sigma [\![\boldsymbol{u}_h^2]\!] \, [\![\phi_h]\!] \, \mathrm{d}S_x, \ \forall \, \phi_h \in Q_h.$$

$$(5c)$$

The initial values can be obtained by a standard projection onto the space Q_h,

$$\Pi_h[r]_{|K} = \frac{1}{|K|} \int_K r \, \mathrm{d}x \ \text{ for any } K \in \mathcal{T}_h,$$

i.e. $(\varrho_{0,h}, \boldsymbol{m}_{0,h}, E_{0,h}) = (\Pi_h[\varrho_0], \Pi_h[\boldsymbol{m}_0], \Pi_h[E_0])$.

Remark 1 The FLM method (5) can be also rewritten in the following per-cell flux formulation

$$D_t \varrho_K + \sum_{\sigma \in \partial K} \frac{|\sigma|}{|K|} F_h(\varrho_h, \boldsymbol{u}_h) = 0,$$

$$D_t \boldsymbol{m}_K + \sum_{\sigma \in \partial K} \frac{|\sigma|}{|K|} (\mathbf{F}_h(\boldsymbol{m}_h, \boldsymbol{u}_h) + \overline{p_h}\boldsymbol{n}) = h^{\alpha-1} \sum_{\sigma \in \partial K} \frac{|\sigma|}{|K|} [\![\boldsymbol{u}_h]\!],$$

$$D_t E_K + \sum_{\sigma \in \partial K} \frac{|\sigma|}{|K|} \left(F_h[E_h, \boldsymbol{u}_h] + (\overline{p_h}\boldsymbol{u}_h + p_h \overline{\boldsymbol{u}_h}) \cdot \boldsymbol{n} \right) = \frac{h^{\alpha-1}}{2} \sum_{\sigma \in \partial K} \frac{|\sigma|}{|K|} [\![\boldsymbol{u}_h^2]\!],$$

for any $K \in \mathcal{T}_h$.

2.2.1 Properties of the FLM Method

For the rigorous convergence analysis of scheme (5) a few important properties are inevitable.

- **Existence of numerical solution.**
  The discrete problem (5) admits a solution $(\varrho_h(t), \boldsymbol{m}_h(t), E_h(t)) \in Q_h \times Q_h \times Q_h$, for any $t \geq 0$. As shown in [9], the result follows from the standard theory of ODEs and sufficiently strong *a priori* bounds.
- **Conservation of discrete mass and energy.**
  In a straightforward way it can be shown that

$$\int_\Omega \varrho_h(t, \cdot) \, \mathrm{d}x = \int_\Omega \varrho_{0,h} \, \mathrm{d}x = \tilde{M}_0 > 0,$$

$$\int_\Omega E_h(t, \cdot) \, \mathrm{d}x = \int_\Omega E_{0,h} \, \mathrm{d}x = \tilde{E}_0 > 0, \ t \geq 0.$$

- **Positivity of the discrete density, pressure and temperature.**
  For any fixed h, the approximate density, pressure and consequently also temperature remain strictly positive on any finite time interval. We refer the reader to [9, Sections 4.3, 4.4] for more details.
- **Discrete entropy inequality.**
  The discrete (renormalized) entropy inequality in the sense of Tadmor is satisfied, cf. [21, 20]. More precisely, it holds that

$$\frac{\mathrm{d}}{\mathrm{d}t} \int_{\mathcal{T}_h} \varrho_h \chi(s_h) \Phi_h \, \mathrm{d}x \geq \sum_{\sigma \in \Sigma_{int}} \int_\sigma U p [\varrho_h \chi(s_h), \boldsymbol{u}_h] [[\Phi_h]] \mathrm{d}S_x +$$

$$+ \sum_{\sigma \in \Sigma_{int}} \int_\sigma \mu_h \left(\overline{\nabla_\varrho(\varrho_h \chi(s_h))} [[\varrho_h]] + \overline{\nabla_p(\varrho_h \chi(s_h))} [[p_h]] \right) [[\Phi_h]] \mathrm{d}S_x,$$

where χ is a non-decreasing, concave, twice continuously differentiable function on R that is bounded from above. For the derivation and proof see [9, Section 3.2].
- **Minimum entropy principle**
  The discrete physical entropy $s_h = \log\left(\vartheta_h^{c_v}/\varrho_h\right)$ attains its minimum at the initial

time, cf. [13, 22], i.e.,

$$s_h(t) \geq s_0, \ t \geq 0, \ \text{where} \ -\infty < s_0 < \min s_h(0).$$

The entropy is either constant or produced over time, thus the second law of thermodynamics holds. See [9, Section 4.2] for more details.

Clearly, the FLM method belongs to the class of invariant domain preserving schemes introduced in [13, 14]. Based on the above properties the following convergence results for the FLM method was proved in [9].

Theorem 1 (Convergence of the FLM method)

Let the initial data $(\varrho_{0,h}, \boldsymbol{m}_{0,h}, E_{0,h})$ satisfy

$$\varrho_{0,h} \geq \underline{\varrho} > 0, \ E_{0,h} - \frac{1}{2}\frac{|\boldsymbol{m}_{0,h}|^2}{\varrho_{0,h}} > 0.$$

Let $(\varrho_h, \boldsymbol{m}_h, E_h) \in Q_h \times Q_h \times Q_h$ be the solution of the scheme (5) such that

$$0 < \beta < 1, \ 0 < \alpha < \frac{4}{3},$$

and

$$0 < \underline{\varrho} \leq \varrho_h(t), \ \vartheta_h(t) \leq \overline{\vartheta} \text{ for all } t \in [0,T] \text{ uniformly for } h \to 0.$$

Then the family of approximate solutions $\{\varrho_h, \boldsymbol{m}_h, E_h\}_{h>0}$ generates a dissipative measure–valued (DMV) solution of the complete Euler system (1) in the sense of [2].

Let us point out that a DMV solution of the Euler system is a time-space parametrized probability measure, i.e. the Young measure. The expected values of density and entropy with respect to this Young measure satisfy the corresponding weak formulation of mass conservation and entropy inequality, respectively. The weak formulation for the expected value of the momentum allows a concentration defect that is controlled by the dissipation in the energy balance. The energy conservation is relaxed and the expected value of the energy dissipates in time, see [2] and [9].

Furthermore, evoking the DMV–strong uniqueness result proved in [2, Theorem 3.3] we obtain the following strong convergence result.

Theorem 2 (Strong convergence of the FLM method)

In addition to the hypotheses of Theorem 1, suppose that the complete Euler system (1) admits a Lipschitz–continuous solution $(\varrho, \boldsymbol{m}, E)$ defined on $[0,T]$.
Then

$$\varrho_h \to \varrho, \ \boldsymbol{m}_h \to \boldsymbol{m}, \ E_h \to E \text{ (strongly) in } L^1((0,T) \times \Omega).$$

In Section 3 we will illustrate numerical behaviour of the FLM method on a series of well-known benchmarks. In what follows we recall the extension of the

FLM method to the finite volume method for the Navier–Stokes–Fourier system introduced in [11]. It turned out that for the convergence analysis of the latter system it is more convenient to work with the temperature formulation instead of the full energy in the last equation of (2).

2.3 Numerical Scheme for the Navier–Stokes–Fourier System

Having introduced the notation in Section 2.1, we now present a semi-discrete finite volume approximation of the Navier–Stokes–Fourier system (2),

$$D_t \varrho_h + \mathrm{div}_h^{\mathrm{up}}(\varrho_h \boldsymbol{u}_h) = 0,$$

$$D_t(\varrho_h \boldsymbol{u}_h) + \mathrm{div}_h^{\mathrm{up}}(\varrho_h \boldsymbol{u}_h, \boldsymbol{u}_h) + \nabla_h p_h = 2\mu \mathrm{div}_h D_h(\boldsymbol{u}_h) + \lambda \nabla_h \mathrm{div}_h \boldsymbol{u}_h,$$

$$c_v D_t(\varrho_h \vartheta_h) + c_v \mathrm{div}_h^{\mathrm{up}}(\varrho_h \vartheta_h, \boldsymbol{u}_h) - \kappa \Delta_h \vartheta_h$$
$$= 2\mu \left| \mathbf{D}_h(\boldsymbol{u}_h) \right|^2 + \lambda \left| \mathrm{div}_h \boldsymbol{u}_h \right|^2 - p_h \mathrm{div}_h \boldsymbol{u}_h.$$

Note that a fully discrete (implicit in time) version of this scheme was analysed in our work [11].

Definition 2 (Finite volume method for NSF) Given the initial values $(\varrho_{0,h}, \boldsymbol{u}_{0,h}, \vartheta_{0,h}) \in Q_h \times Q_h \times Q_h$, we seek a piecewise constant approximation $(\varrho_h, \boldsymbol{u}_h, \vartheta_h) \in Q_h \times Q_h \times Q_h$ which solves at any time $t \in (0, T]$ the following equations:

$$\int_\Omega D_t \varrho_h \, \phi_h \, \mathrm{d}x - \sum_{\sigma \in \Sigma_{int}} \int_\sigma F_h(\varrho_h, \boldsymbol{u}_h) \, [\![\phi_h]\!] \, \mathrm{d}S_x = 0, \ \forall \phi_h \in Q_h, \qquad (6\mathrm{a})$$

$$\int_\Omega D_t(\varrho_h \boldsymbol{u}_h) \cdot \boldsymbol{\phi}_h \, \mathrm{d}x - \sum_{\sigma \in \Sigma_{int}} \int_\sigma \mathbf{F}_h(\varrho_h \boldsymbol{u}_h, \boldsymbol{u}_h) \cdot [\![\boldsymbol{\phi}_h]\!] \, \mathrm{d}S_x - \int_\Omega p_h \mathrm{div}_h \boldsymbol{\phi}_h \, \mathrm{d}x$$
$$= -2\mu \int_\Omega D_h(\boldsymbol{u}_h) : \nabla_h \boldsymbol{\phi}_h \, \mathrm{d}x - \lambda \int_\Omega \mathrm{div}_h \boldsymbol{u}_h \mathrm{div}_h \boldsymbol{\phi}_h \, \mathrm{d}x, \ \forall \boldsymbol{\phi}_h \in Q_h, \quad (6\mathrm{b})$$

$$c_v \int_\Omega D_t(\varrho_h \vartheta_h) \, \phi_h \, \mathrm{d}x - c_v \sum_{\sigma \in \Sigma_{int}} \int_\sigma F_h(\varrho_h \vartheta_h, \boldsymbol{u}_h) \, [\![\phi_h]\!] \, \mathrm{d}S_x - \kappa \int_\Omega \Delta_h \vartheta_h \, \phi_h \, \mathrm{d}x$$
$$= \int_\Omega \left(2\mu \left| \mathbf{D}_h(\boldsymbol{u}_h) \right|^2 + \lambda \left| \mathrm{div}_h \boldsymbol{u}_h \right|^2 - p_h \mathrm{div}_h \boldsymbol{u}_h \right) \phi_h \, \mathrm{d}x, \ \forall \phi_h \in Q_h. \quad (6\mathrm{c})$$

Remark 2 Let us point out that the $h^{\alpha-1}$-terms in (5b) and (5c) yield an additional diffusion and make the FLM method a particular vanishing viscosity approximation of the Euler system. Since the physical viscosity is naturally included in the Navier–Stokes–Fourier system, we do not need to include the additional diffusion in (6).

Remark 3 The numerical scheme (6) can be also rewritten in the usual finite volume formulation for any $K \in \mathcal{T}_h$,

$$D_t \varrho_K + \sum_{\sigma \in \partial K} \frac{|\sigma|}{|K|} F_h(\varrho_h, \boldsymbol{u}_h) = 0,$$

$$D_t(\varrho \boldsymbol{u})_K + \sum_{\sigma \in \partial K} \frac{|\sigma|}{|K|} \left(\mathbf{F}_h(\varrho_h \boldsymbol{u}_h, \boldsymbol{u}_h) + \overline{p_h} \boldsymbol{n} \right)$$

$$= \sum_{\sigma \in \partial K} \frac{|\sigma|}{|K|} \left(2\mu \overline{D_h(\boldsymbol{u}_h)} \cdot \boldsymbol{n} + \lambda \overline{\mathrm{div}_h \boldsymbol{u}_h} \boldsymbol{n} \right),$$

$$c_v D_t(\varrho \vartheta)_K + \sum_{\sigma \in \partial K} \frac{|\sigma|}{|K|} \left(c_v F_h(\varrho_h \vartheta_h, \boldsymbol{u}_h) - \kappa \frac{[\![\vartheta_h]\!]}{d_\sigma} \right)$$

$$= \sum_{\sigma \in \partial K} \frac{|\sigma|}{|K|} \left(2\mu \, |\mathbf{D}_h(\boldsymbol{u}_h)|_K^2 + \lambda \, |\mathrm{div}_h \boldsymbol{u}_h|_K^2 - p_K (\mathrm{div}_h \boldsymbol{u}_h)_K \right).$$

2.3.1 Properties of the FV Method for NSF

Analogously as in the inviscid case for the convergence analysis it is fundamental that our numerical scheme fulfils some invariant domain preserving properties. In [11] we have proved the following:

- **Conservation of discrete mass.**
  One can easily show that

$$\int_\Omega \varrho_h(t, \cdot) \, \mathrm{d}x = \int_\Omega \varrho_{0,h} \, \mathrm{d}x = \tilde{M}_0 > 0, \ t \geq 0.$$

- **Non-negativity of the discrete density.**
  The approximate density remains non-negative on any finite time interval.
- **Discrete total energy dissipation.**
  Let $(\varrho_h, \boldsymbol{u}_h, \vartheta_h) \in Q_h \times Q_h \times Q_h$ be a solution to (6). Then

$$E_h(t) \leq E_0, \ t \geq 0,$$

  where
$$E_h(t) = \int_\Omega \left(\frac{1}{2} \varrho_h(t) |\boldsymbol{u}_h(t)|^2 + c_v \varrho_h(t) \vartheta_h(t) \right) \mathrm{d}x.$$

  See [11, Theorem 3.1] for the proof.
- **Discrete entropy inequality.**
  The scheme (6) is entropy stable. It holds that

$$\int_\Omega D_t \left(\varrho_h s_h\right) \, \mathrm{d}x \geq - \int_\Omega \kappa \nabla_{\mathcal{D}} \vartheta_h \cdot \nabla_{\mathcal{D}} \left(\frac{1}{\vartheta_h}\right) \, \mathrm{d}x$$
$$+ \int_\Omega \frac{1}{\vartheta_h} \left(2\mu |\mathbf{D}(\boldsymbol{u}_h)|^2 + \lambda |\mathrm{div}_h \boldsymbol{u}_h|^2\right) \, \mathrm{d}x,$$

see [11, Lemma 3.4].

Remark 4 Note that the above properties shown in [11] for a fully discrete implicit in time version of scheme (6) can be proven in a straightforward manner for the semi-discrete scheme presented here.

The structure preserving properties listed above, together with the assumptions on uniform boundedness of the discrete density and temperature, are sufficient to derive suitable *a priori* estimates and consistency formulation of scheme (6) which are inevitable for the convergence of its solutions. We now recall the convergence results proved in [11].

Theorem 3 (Convergence of the FV method for NSF)

Let the initial data satisfy the assumptions

$$0 < \underline{\varrho} \leq \varrho_{0,h} \leq \overline{\varrho}, \ 0 < \underline{\vartheta} \leq \vartheta_{0,h} \leq \overline{\vartheta}, \ \|\boldsymbol{u}_{0,h}\|_{L^2} \leq \overline{u},$$

for some positive constants $\underline{\varrho}, \overline{\varrho}, \underline{\vartheta}, \overline{\vartheta}, \overline{u}$. Let $(\varrho_h, \vartheta_h, \boldsymbol{u}_h) \in Q_h \times Q_h \times Q_h$ be the solution of the finite volume scheme (6), satisfying the assumptions

$$0 < \underline{\varrho} \leq \varrho_h(t) \leq \overline{\varrho}, 0 < \underline{\vartheta} \leq \vartheta_h(t) \leq \overline{\vartheta} \text{ uniformly for } h \to 0, \text{ and all } t \in (0,T).$$

Then the family $\{\varrho_h, \vartheta_h, \boldsymbol{u}_h, \mathbf{D}_h(\boldsymbol{u}_h), \nabla_{\mathcal{D}} \vartheta_h\}_{h>0}$ generates a DMV solution of the Navier–Stokes–Fourier system (2) in the sense of [3].

Analogously as for the inviscid flows a DMV solution is the Young measure. Expected values of density, momentum, energy and entropy satisfy appropriate generalized formulation of (2). Further, applying the DMV–strong uniqueness principle established in [3, Theorem 6.1] and [11, Theorem 5.5] we have the following strong convergence result.

Theorem 4 (Strong convergence of the FV method for NSF)

In addition to the hypotheses of Theorem 3 assume that $\{\mathcal{V}_{t,x}\}_{(t,x) \in (0,T) \times \Omega}$ is a DMV solution of the Navier–Stokes–Fourier system (2) in the sense of [3] such that

$$\mathcal{V}_{t,x} \left\{ 0 < \underline{\varrho} \leq \varrho \leq \overline{\varrho}, \ \vartheta \leq \overline{\vartheta}, \ |\boldsymbol{u}| \leq \overline{u} \right\} = 1 \text{ for a.a. } (t,x) \in (0,T) \times \Omega \quad (7)$$

for some constants $\underline{\varrho}, \overline{\varrho}, \overline{\vartheta}$, and $\overline{\boldsymbol{u}}$. Let, moreover,

$$\mathcal{V}_{0,x} = \delta_{\varrho_0(x), \vartheta_0(x), \boldsymbol{u}_0(x)} \quad \text{for a.a. } x \in \Omega,$$

where $(\varrho_0, \vartheta_0, \boldsymbol{u}_0)$ belongs to the regularity class

$$\varrho_0, \vartheta_0 \in W^{3,2}(\Omega), \ \varrho_0, \ \vartheta_0 > 0 \ in \ \Omega, \ \boldsymbol{u}_0 \in W_0^{3,2}(\Omega; R^3). \tag{8}$$

Finally, suppose that the Navier–Stokes–Fourier system (2) *is endowed with the initial data* $(\varrho_0, \vartheta_0, \boldsymbol{u}_0)$ *satisfying* (8). *Let* $(\varrho_h, \vartheta_h, \boldsymbol{u}_h)$ *be the solution of the finite volume scheme* (6), *and in addition,*

$$|\boldsymbol{u}_h(t)| \leq \overline{u} \ uniformly \ for \ h \to 0 \ and \ all \ t \in (0, T).$$

Then

$$\varrho_h \to \varrho \ (strongly) \ in \ L^p \left((0, T) \times \Omega \right),$$
$$\vartheta_h \to \vartheta \ (strongly) \ in \ L^p \left((0, T) \times \Omega \right),$$
$$\boldsymbol{u}_h \to \boldsymbol{u} \ (strongly) \ in \ L^p \left((0, T) \times \Omega; R^d \right), \ p \in [1, \infty),$$

where $(\varrho, \vartheta, \boldsymbol{u})$ *is a strong (classical) solution of the Navier–Stokes–Fourier system.*

3 Numerical Experiments

In this section we demonstrate the performance of both finite volume methods, the FLM method (5) for the Euler equations, and the finite volume method (6) for the Navier–Stokes–Fourier equations.

For time discretization we use the forward finite differences which yield the explicit finite volume scheme for the Euler system. Diffusive fluxes in the Navier–Stokes–Fourier equations are approximated by the backward finite differences and thus implicitly in time. For stability reasons, we set the time step as $\delta t = \min\{\delta t_a, \delta t_b\}$ in each sub-iteration. The first term arises from the CFL stability condition: $\delta t_a = \text{CFL} \, h / \max\{|\boldsymbol{u}| + c\}, \ c = \sqrt{\vartheta}$. In our numerical simulations we set CFL $= 0.5$ if not explicitly claimed otherwise. The second term is due to the parabolic regularization: $\delta t_b = h^{1-\beta}/(2d)$.

3.1 Numerical Experiments for the FLM Method

3.1.1 Experimental Order of Convergence (EOC)

We aim to validate the theoretical result on the convergence of $\varrho, \boldsymbol{m}, E$ presented in Theorem 2 by computing the corresponding norms of numerical errors

$$\|e_f\| = \frac{\|f - f_{ref}\|_{L_t^1 L_x^1}}{\|f_{ref}\|_{L_t^1 L_x^1}}, \quad f \in \{\varrho, \boldsymbol{m}, E\},$$

where $L_t^1 L_x^1$ is a shortening for $L^1(0, T; L^1(\Omega)) \equiv L^1((0, T) \times \Omega)$. Analogous notation is used for other Bochner spaces below. Additionally, we also provide the numerical errors of the velocity $\boldsymbol{u}$ in $L_t^2 L_x^2$–norm and pressure p in $L_t^\infty L_x^1$–norm. The reference solution is the exact solution to (1)

$$\varrho_{ref} = 2 + \cos(2\pi x), \quad \boldsymbol{u}_{ref} = \frac{\sin(\pi t)}{2 + \cos(2\pi x)} \begin{pmatrix} 1 \\ -1 \end{pmatrix},$$

$$p_{ref} = (2 + \cos(2\pi x))(2 + \sin(2\pi x)), \qquad x \in [0, 1]. \tag{9}$$

Setting $\gamma = 1.4$, $\alpha = 1.3$, $\beta = 0.2$ and CFL = 0.6, we observe the first order convergence rate for the FLM method, see Table 1.

Table 1 Relative errors and EOC for the FLM method (5) at time $t = 0.1$.

h	$\|e_\varrho\|$	EOC	$\|e_{\boldsymbol{m}}\|$	EOC	$\|e_E\|$	EOC	$\|e_{\boldsymbol{u}}\|$	EOC	$\|e_p\|$	EOC
1/32	9.00e-03	1.13	4.15e-02	1.10	1.21e-02	1.13	5.75e-02	1.06	1.94e-02	1.12
1/64	4.05e-03	1.15	1.88e-02	1.14	5.40e-03	1.16	2.65e-02	1.12	8.74e-03	1.15
1/128	1.81e-03	1.16	8.36e-03	1.17	2.41e-03	1.16	1.20e-02	1.14	3.94e-03	1.15
1/256	8.07e-04	1.17	3.71e-03	1.17	1.08e-03	1.16	5.41e-03	1.15	1.78e-03	1.15

3.1.2 1D Benchmark Problems

We test one-dimensional Riemann problems studied in [15, 23] with the initial data

$$(\varrho, u, p) = \begin{cases} (\varrho_L, u_L, p_L) & \text{if } 0 \leq x < x_m, \\ (\varrho_R, u_R, p_R) & \text{if } x_m \leq x \leq 1, \end{cases}$$

and details presented in Table 2.

Table 2 Initial data of 1D tests.

Test	ϱ_L	u_L	p_L	ϱ_R	u_R	p_R	T_{max}	x_m
1	1.0	-2.0	0.4	1.0	2.0	0.4	0.15	0.5
2	1.0	0.0	1000.0	1.0	0.0	0.01	0.012	0.5
3	1.4	0.0	1.0	1.0	0.0	1.0	2.0	0.5
4	1.4	0.1	1.0	1.0	0.1	1.0	2.0	0.5

Test 1 has a weak solution consisting of two rarefaction waves and it is typically used for checking the positivity of density; Test 2 is designed for strong shock; Test 3 and 4 are designed to capture stationary contact waves. We set $\gamma = 1.4$, $\beta = 0.2$ and aim to show the numerical performance of the scheme (5) on the domain $\Omega = [0, 1]$

with mesh size $h = 1/400$. First, we present in Figure 2 the results of numerical simulations for different choices of α, that is the parameter appearing in the artificial diffusion terms in equations (5b) and (5c). Secondly, we show in Figure 3 the comparison of the numerical solutions obtained by the FLM method with that of the HLL finite volume method [23].
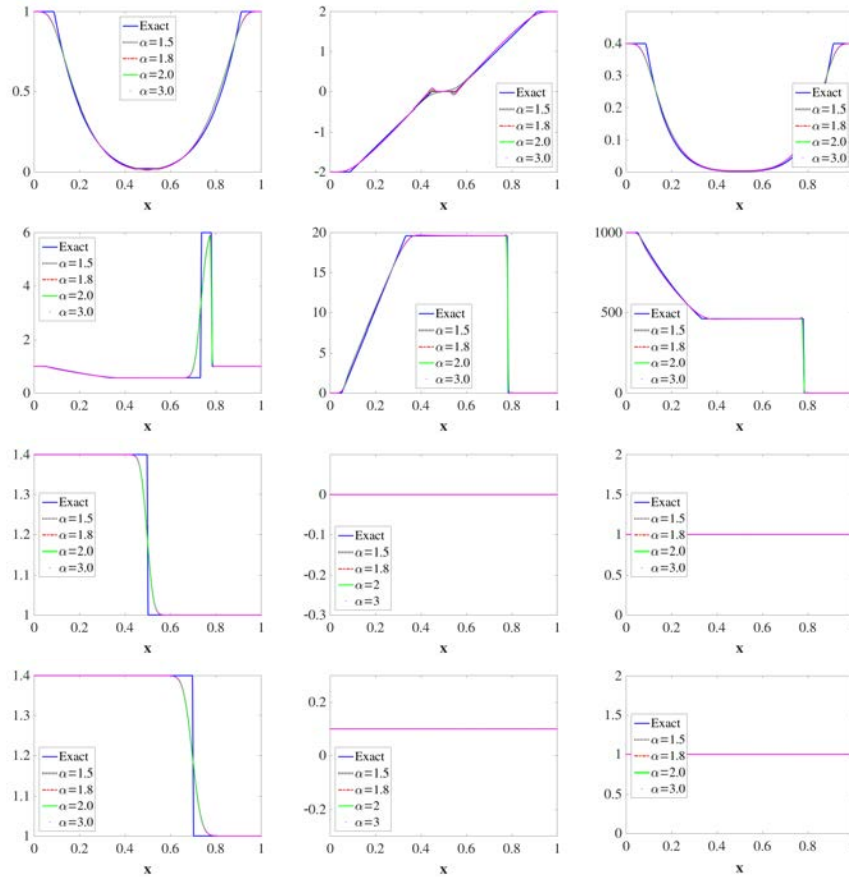

Fig. 2 1D tests: from top to bottom are Tests 1 to 4, from left to right solutions of $\varrho, \boldsymbol{u}, p$.
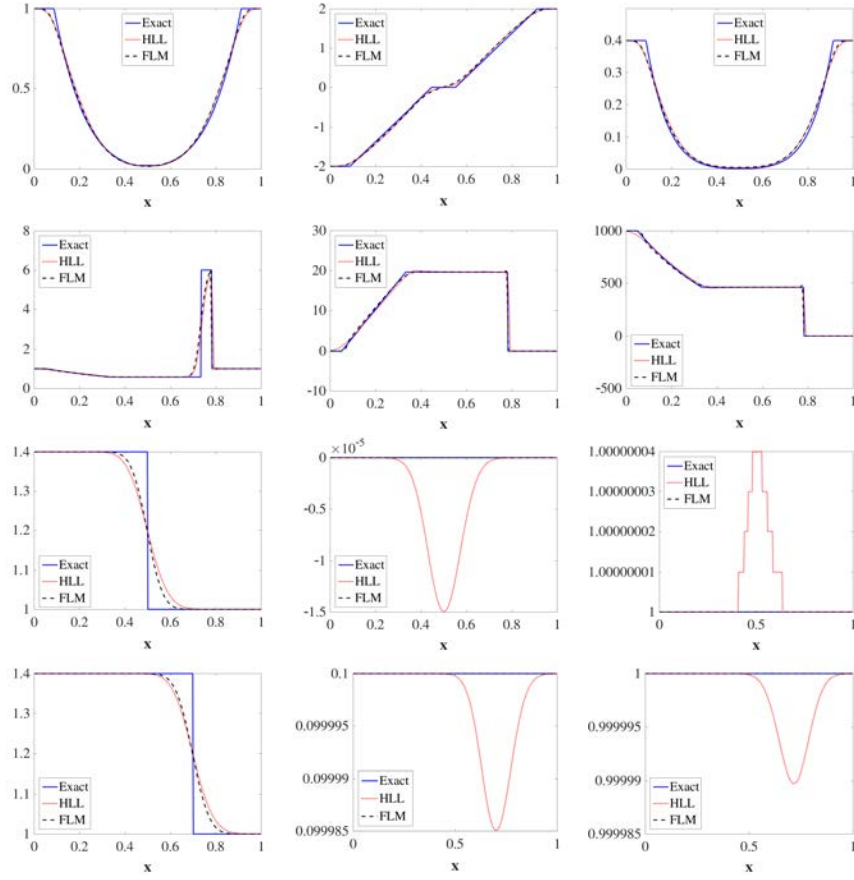
Fig. 3 1D tests: from top to bottom are Tests 1 to 4, from left to right solutions of ϱ, $\boldsymbol{u}$, p.

3.1.3 2D Benchmark Problems

Now we test the two-dimensional Riemann problems studied in [15, 16, 17] with $\Omega = [-1, 1]^2$. Boundary values are obtained by extrapolation of conservative variables $(\varrho, \boldsymbol{m}, E)$.

Test 1: circular two-dimensional Sod problem with the initial data

$$(\varrho, u_1, u_2, p) = \begin{cases} (1.0, 0, 0, 1.0), & |x| < 0.4, \\ (1.0, 0, 0, 0.1), & \text{else.} \end{cases}$$

Figure 4 displays the contour lines of the numerical solution of density, velocity components, and pressure at time $t = 0.2$ which are in a very good agreement with the results presented in literature, cf., e.g., [23].
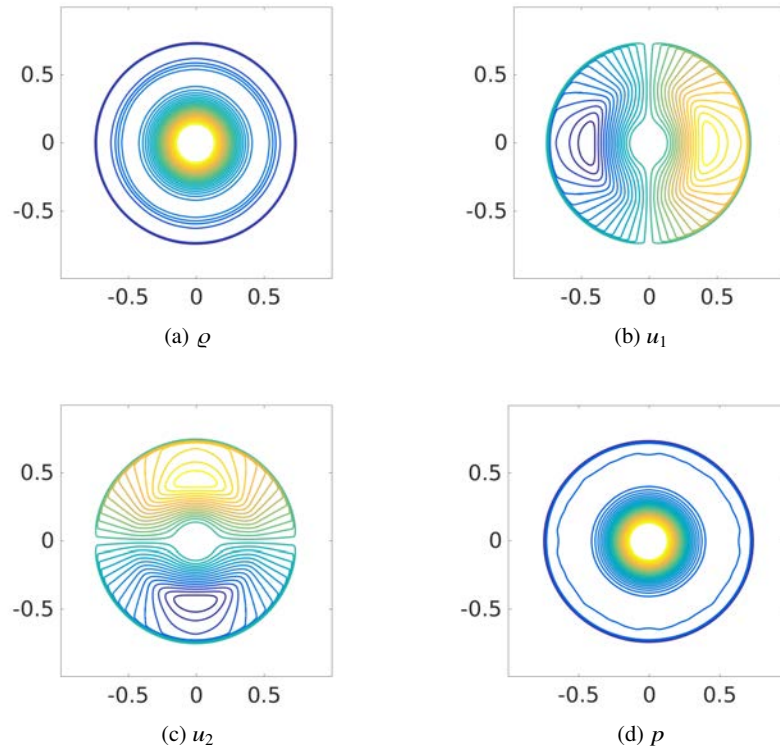

(a) ϱ

(b) u_1

(c) u_2

(d) p

Fig. 4 Test 1: Sod problem solution on rectangular mesh $h_x = h_y = 0.05$ with $\alpha = 1.5, \beta = 0.2$ at time $t = 0.2$.

Test 2: two-dimensional benchmark Riemann problem consisting of two moving shocks and two standing slip lines. The initial values are set as

$$(\varrho, u_1, u_2, p) = \begin{cases} (0.5313, 0, 0.7276, 0.4), & x > 0, y > 0, \\ (1.0, 0.7276, 0, 1.0), & x < 0, y > 0, \\ (0.8, 0, 0, 1.0), & x < 0, y < 0, \\ (1.0, 0, 0.7276, 1.0), & x > 0, y < 0. \end{cases}$$

Figure 5 shows the numerical solution for density and pressure for different CFL numbers. Numerical solutions obtained by the FLM method are in good agreement with the results presented in literature, see, e.g., [16].
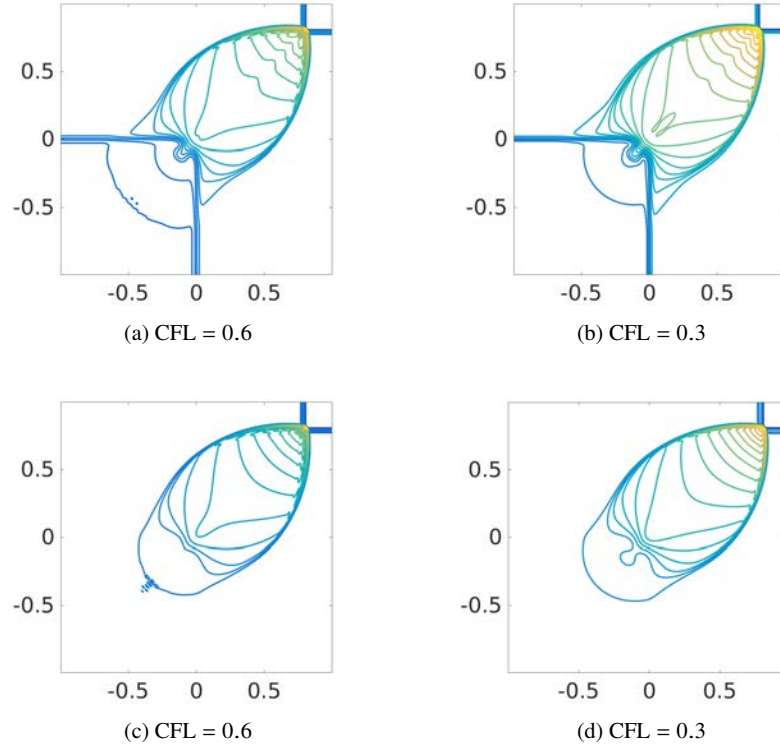

(a) CFL = 0.6

(b) CFL = 0.3

(c) CFL = 0.6

(d) CFL = 0.3

Fig. 5 Test 2: solution of ϱ (upper row) and p (lower row) on rectangular mesh $h_x = h_y = 0.05$ with $\alpha = 1.5, \beta = 0.5$ at time $t = 0.52$.

Test 3: two-dimensional Riemann problem with the initial condition

$$(\varrho, u_1, u_2, p) = \begin{cases} (1.1, 0, 0, 1.1), & x > 0, y > 0, \\ (0.5065, 0, 0.8939, 0.35), & x < 0, y > 0, \\ (1.1, 0.8939, 0.8939, 1.1), & x < 0, y < 0, \\ (0.5065, 0, 0.8939, 0.35), & x > 0, y < 0. \end{cases}$$

In this configuration there are two forward moving shocks and two backward moving shocks. Figure 6 depicts the contour lines of the numerical solution of density, velocity components, and pressure at time $t = 0.25$. We can again confirm that the numerical solution is in good agreement with the results presented in the literature, cf., e.g., [16].
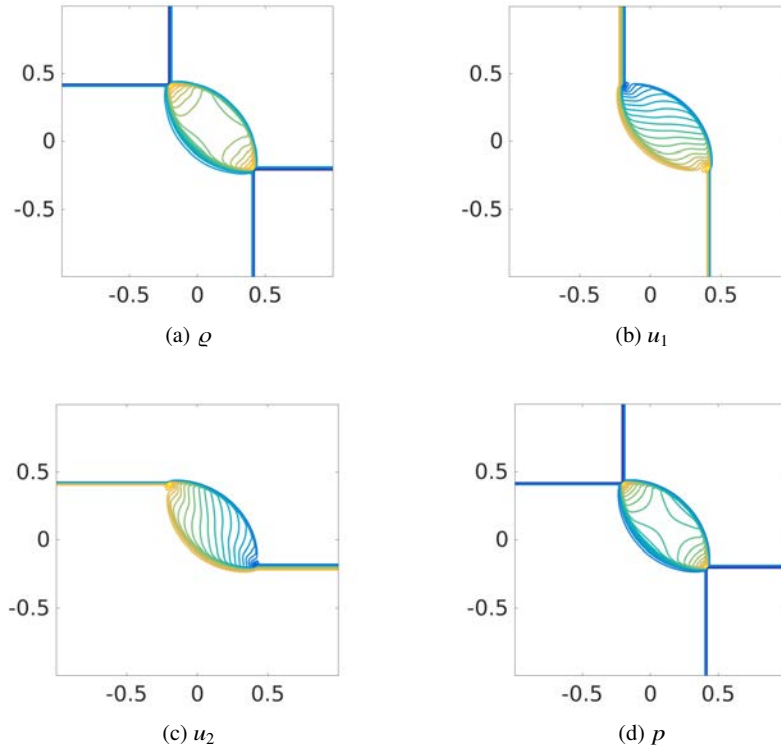

(a) ϱ (b) u_1

(c) u_2 (d) p

Fig. 6 Test 3: solution of ϱ, u_1, u_2, and p on rectangular mesh $h_x = h_y = 0.05$ at time $t = 0.25$.

3.2 Numerical Experiments for the FV Method for NSF

3.2.1 Experimental Order of Convergence (EOC)

Our aim in this section is to validate theoretical results on the convergence of ϱ, $\boldsymbol{u}$, ϑ presented in Theorem 4 by computing the numerical errors

$$\|e_f\| = \frac{\|f - f_{ref}\|_{L_t^q L_x^q}}{\|f_{ref}\|_{L_t^q L_x^q}}, \quad f \in \{\varrho, \boldsymbol{u}, \vartheta\}, \ q = 1, 2.$$

Here the reference solution is the same as in (9). Thus, we have a manufactured exact solution with a suitable external force in the momentum and energy equation. Setting $\mu = \lambda = \kappa = 1$ and CFL $= \beta = 0.6$, we observe the first order convergence rate for the scheme (6), see Table 3. We can observe first order convergence on rectangular as well as triangular mesh.

Table 3 Relative errors and EOC for the FV method (6) for NSF at time $t = 0.2$.

h	$\|e_\varrho\|$	EOC	$\|e_{\boldsymbol{u}}\|$	EOC	$\|e_\vartheta\|$	EOC	$\|e_\varrho\|$	EOC	$\|e_{\boldsymbol{u}}\|$	EOC	$\|e_\vartheta\|$	EOC
	$L^1((0,T) \times \Omega)$-norm						$L^2((0,T) \times \Omega)$-norm					
	rectangular mesh											
32	2.09e-02	–	2.24e-02	–	1.27e-02	–	2.52e-02	–	2.71e-02	–	1.49e-02	–
64	9.51e-03	1.14	1.06e-02	1.08	5.78e-03	1.13	1.15e-02	1.12	1.31e-02	1.05	6.84e-03	1.12
128	4.27e-03	1.16	4.87e-03	1.12	2.60e-03	1.15	5.21e-03	1.15	6.10e-03	1.10	3.09e-03	1.15
256	1.90e-03	1.16	2.21e-03	1.14	1.16e-03	1.16	2.34e-03	1.16	2.80e-03	1.12	1.38e-03	1.16
512	8.49e-04	1.17	9.98e-04	1.15	5.20e-04	1.16	1.05e-03	1.16	1.27e-03	1.14	6.19e-04	1.16
	triangular mesh											
1/32	9.17e-03	–	1.23e-02	–	4.90e-03	–	1.10e-02	–	1.60e-02	–	5.82e-03	–
1/64	4.02e-03	1.19	6.68e-03	0.89	2.43e-03	1.01	4.83e-03	1.18	8.79e-03	0.87	2.92e-03	0.99
1/128	1.78e-03	1.18	4.10e-03	0.70	1.20e-03	1.02	2.13e-03	1.18	5.44e-03	0.69	1.45e-03	1.01
1/256	7.92e-04	1.17	2.99e-03	0.46	5.87e-04	1.03	9.50e-04	1.17	3.94e-03	0.46	7.19e-04	1.01
1/512	3.56e-04	1.15	2.53e-03	0.24	2.89e-04	1.02	4.27e-04	1.15	3.31e-03	0.25	3.57e-04	1.01

3.2.2 2D Benchmark Problems

Test 4: Circular shock problem.
We again test the two-dimensional Sod problem using the same initial data as in the first experiment of Section 3.1.3 with $\mu = \lambda = \kappa = 0.001$ and CFL $= \beta = 0.6$. The contour lines of the numerical solutions are shown in Figure 7. Small viscosity effects can be noticed but overall the numerical solutions for inviscid and viscous case are similar as expected.
Test 5: Gresho Vortex problem with the initial data [15]

$$(u, p)(r) = \begin{cases} (5r, \ 5 + 12.5r^2) & r < 0.2, \\ (2 - 5r, \ 9 - 4\ln 0.2 + 12.5r^2 - 20r + 4\ln r) & 0.2 \le r < 0.4, \\ (0, \ 3 + 4\ln 2) & r > 0.4. \end{cases}$$

Figure 8 displays the contour lines of the numerical solutions obtained by the scheme (6) with the parameters $\mu = \lambda = \kappa = 0.01$, and CFL $= \beta = 0.6$ at time $t = 0.2$.
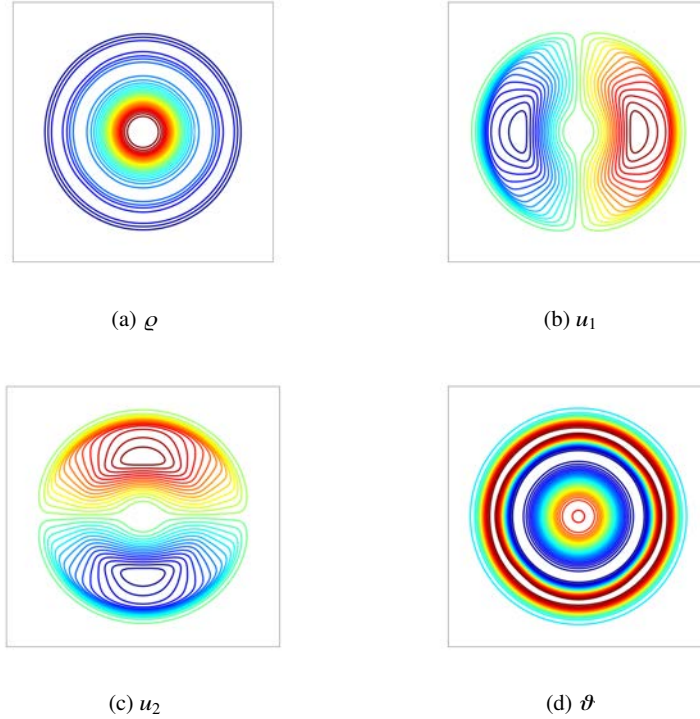

(a) ϱ

(b) u_1

(c) u_2

(d) ϑ

Fig. 7 Test 4: Circular shock solution on rectangular mesh $h_x = h_y = 0.05$ at time $t = 0.2$.

Conclusion

We have presented behaviour and performance of two new convergent finite volume methods for compressible fluids, both inviscid and viscous. These new finite volume methods satisfy some important invariant domain preserving properties, such as the minimum entropy principle, mass and energy conservation, positivity preservation, total energy dissipation and entropy production. These are crucial for showing the
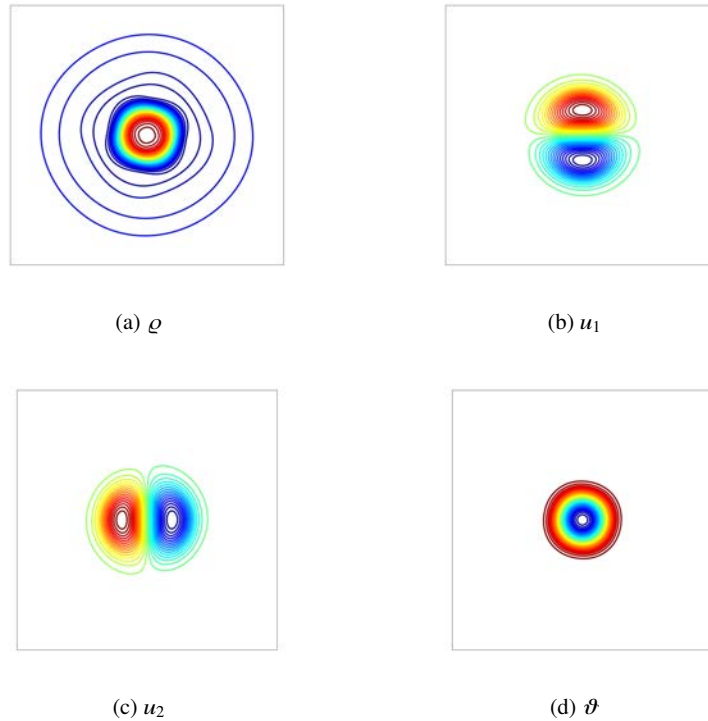
(a) ϱ

(b) u_1

(c) u_2

(d) ϑ

Fig. 8 Test 5: Gresho vortex solution on rectangular mesh $h_x = h_y = 0.05$ at time $t = 0.2$.

stability and consistency of the schemes. In the framework of a nonlinear version of the Lax-equivalence theorem, see [9, 11], these properties directly imply the strong convergence of numerical solutions to a strong solution on its lifespan. Our numerical experiments presented in Section 3 confirm these theoretical convergence results.

References

1. M. Ben-Artzi, J. Li, and G. Warnecke. A direct Eulerian GRP scheme for compressible fluid flows. *J. Comput. Phys.* **218**(1): 19–43, 2006.

2. J. Březina and E. Feireisl. Measure-valued solutions to the complete Euler system. *J. Math. Soc. Jpn.* **70**(4): 1227–1245, 2018.
3. J. Březina, E. Feireisl, and A. Novotný. Stability of strong solutions to the Navier–Stokes–Fourier system. CAS preprint, 2018.
4. P. G. Ciarlet. The Finite Element Method for Elliptic Problems. *Classics in Applied Mathematics, Society for Industrial and Applied Mathematics*, 2002.
5. B. Cockburn and C. Shu. TVB Runge-Kutta local projection discontinuous Galerkin finite element method for conservation laws. II. General framework. *Math. Comp.* **52**(186): 411–435, 1989.
6. V. Dolejší and M. Feistauer. Discontinuous Galerkin method. *volume 48 of Springer Series in Computational Mathematics*, Springer, Cham, 2015. xiv+572 pp. Analysis and applications to compressible flow.
7. R. Eymard, T. Gallouët, and R. Herbin. Finite volume methods. *Handbook of numerical analysis* **7**: 713–1018, 2000.
8. E. Feireisl, P. Gwiazda, A. Świerczewska-Gwiazda, and E. Wiedemann. Dissipative measure-valued solutions to the compressible Navier–Stokes system. *Calc. Var. Partial Dif.* **55**(6): 55–141, 2016.
9. E. Feireisl, M. Lukáčová-Medviďová, and H. Mizerová. A finite volume scheme for the Euler system inspired by the two velocities approach. *Numer. Math. 2019.* doi:10.1007/s00211-019-01078-y
10. E. Feireisl, M. Lukáčová-Medviďová, H. Mizerová, and B. She. Convergence of a finite volume scheme for the compressible Navier–Stokes system. *ESAIM: M2AN* **53**(6): 1957-1979, 2019.
11. E. Feireisl, M. Lukáčová-Medviďová, H. Mizerová, and B. She. On the convergence of a finite volume scheme for the compressible Navier–Stokes–Fourier system. arXiv preprint No. 1903.08526
12. S. K. Godunov. A difference method for numerical calculation of discontinuous solutions of the equations of hydrodynamics. *Mat. Sb. (N.S.)* **47**(89): 3 271–306, 1959.
13. J. L. Guermond and B. Popov. Viscous regularization of the Euler equations and entropy principles. *SIAM J. Appl. Math.* **74**(2): 284–305, 2014.
14. J. L. Guermond and B. Popov. Invariant domains and first-order continuous finite element approximation for hyperbolic systems. *SIAM J. Num. Anal.* **54**: 2466–2489, 20165.
15. R. Liska and B. Wendroff. Comparison of Several Difference Schemes on 1D and 2D Test Problems for the Euler Equations. *SIAM J. Sci. Comput.* **25**(3): 995–1017, 2003.
16. M. Lukáčová-Medviďová, J. Saibertová, and G. Warnecke. Finite Volume Evolution Galerkin Methods for Nonlinear Hyperbolic Systems. *J. Comput. Phys.* **183**(2): 533–562, 2002.
17. C. W. Schulz-Rinne, J. P. Collins, and H. M. Glaz. Numerical Solution of the Riemann Problem for Two–Dimensional Gas Dynamics. *SIAM J. Sci. Comput.* **14**(6): 1394–1414, 1993.
18. H. Shen, C. Y. Wen, and D. L.Zhang. A characteristic space-time conservation element and solution element method for conservation laws. *J. Comput. Phys.* **288**: 101–118, 2015.
19. C. Shu and S. Osher. Efficient implementation of essentially nonoscillatory shock-capturing schemes. *J. Comput. Phys.* **77**(2): 439–471, 1988.
20. E. Tadmor. Entropy stability theory for difference approximations of nonlinear conservation laws and related time dependent problems. *Acta Numer.* **12**: 451–512, 2003.
21. E. Tadmor. The numerical viscosity of entropy stable schemes for systems of conservation laws. *Math. Comp.* **49**(179): 91–103, 1987.
22. E. Tadmor. Minimum entropy principle in the gas dynamic equations. *Appl. Num. Math.* **2**: 211–219, 1986.
23. E. F. Toro. Riemann solvers and numerical methods for fluid dynamics. A practical introduction. Third edition. Springer-Verlag, Berlin, 2009. xxiv+724 pp.
24. E. VanderZee, A. N. Hirani, D. Guoy, and E. A. Ramos. Well-centered triangulation. *SIAM J. Sci. Comput.* **31**(6): 4497–4523, 2010.
25. K. Xu, C. Kim, L. Martinelli, and A. Jameson. BGK–based schemes for the simulation of compressible flow. *Int. J. Comput. Fluid Dyn.* **7**(3): 213–235, 1996.